Published in final edited form as:
Biochem Pharmacol. 2012 August 1; 84(3): 383–390. doi:10.1016/j.bcp.2012.04.018.

Residue Ile89 in Human Plasma Membrane Monoamine Transporter influences its Organic Cation Transport Activity and Sensitivity to Inhibition by Dilazep

Horace T.B. Ho[a], **Li Xia**[a,1], and **Joanne Wang**[a,*]

Horace T.B. Ho: horaceho@u.washington.edu; Li Xia: Li.Xia@fda.hhs.gov; Joanne Wang: jowang@u.washington.edu

[a]Department of Pharmaceutics, University of Washington, Seattle, Washington 98195, USA

Abstract

Plasma membrane monoamine transporter (PMAT) is a polyspecific organic cation transporter belonging to the equilibrative nucleoside transporter (ENT) family. Despite its distinct substrate specificity from the classic nucleoside transporters ENT1 and 2, PMAT appears to share similar protein architecture with ENT1/2 and retains low affinity binding to classic ENT inhibitors such as nitrobenzylmercaptopurine riboside (NBMPR) and the coronary vasodilators dilazep and dipyridamole. Here we investigated the role of residue Ile89, a position known to be important for ENT interaction with dilazep, dipyridamole, and nucleoside substrates, in PMAT transport function and its interaction with classic ENT inhibitors using Madin-Darby canine kidney (MDCK) cells stably expressing human PMAT. Substitution of Ile89 in PMAT with Met, the counterpart residue in ENT1, resulted in normal plasma membrane localization and protein expression. Transport kinetic analysis revealed that I89M mutant had a 2.7-fold reduction in maximal transport velocity (Vmax) with no significant change in apparent binding affinity (Km) towards the prototype PMAT substrate 1-methyl-4-phenylpyridinium (MPP^+), suggesting that I89 is an important determinant for the catalytic activity of PMAT. Dose-dependent inhibition studies further showed that the I89M mutation significantly increased PMAT's sensitivity to dilazep by 2.5 fold without affecting its sensitivity to dipyridamole and NBMPR. Located at the extracellular end of transmembrane domain 1 of PMAT, I89 may occupy an important position close to the substrate permeation pathway and may be involved in direct interaction with the vasodilator dilazep.

Keywords

PMAT; SLC29 family; ENT4; Dilazep; Dipyridamole

1. Introduction

The human solute carrier 29 (SLC29) family is represented by four members that play important roles in cellular uptake of nutrients, signaling molecules and therapeutic drugs

*Corresponding author. Joanne Wang, Department of Pharmaceutics, Health Sciences Building, Room H272J, University of Washington, 1959 NE Pacific St, Seattle, Washington 98195, USA. Telephone: +1 206-221-6561. Fax: +1 206-543-3204. jowang@u.washington.edu.

[1]Present address: Division of Bioequivalence II, Office of Generic Drugs, FDA, Rockville, MD, 20855, USA.

[1,2]. SLC29A1 and SLC29A2 encode the classic equilibrative nucleoside transporters 1 and 2 (ENT1 and ENT2), which mediate facilitative transport of purine and pyrimidine nucleosides and their structural analogs [1,2]. ENT1 and ENT2 are involved in nucleoside salvage pathways, regulation of purinergic signaling, and cellular disposition of nucleoside analogs used in anticancer, antiviral and immunosuppressive therapies [1,2]. The third member, ENT3 (SLC29A3), also transports nucleosides and nucleoside analogs, and appears to function mainly as an intracellular transporter [3,4]. The fourth member, SLC29A4, was cloned and characterized in our laboratory as the plasma membrane monoamine transporter (PMAT) [5]. PMAT (also named ENT4) is different from ENT1-3 in that with the exception of adenosine, PMAT does not significantly transport nucleosides and nucleoside analogs [5,6]. Instead, it functions as a polyspecific organic cation transporter that robustly transports a wide range of structurally diverse organic cations [5,7] such as the neurotoxin 1-methyl-4-phenylpyridinium (MPP^+), the monoamine neurotransmitters (e.g. serotonin, dopamine), and the anti-diabetic drug metformin [8], which are also transported by organic cation transporters (OCTs) in the SLC22 family [9,10]. We previously showed that PMAT is an electrogenic transporter and PMAT-mediated organic cations transport is dependent on both membrane potential and pH [5,11,12]. In humans, PMAT mRNA is most strongly expressed in the brain, but transcripts are also found in other organs such as the kidney, heart, and small intestine [5,8,13]. Interestingly, PMAT was found to be predominantly expressed in the visceral glomerular epithelial cells (podocytes) in human and rat kidneys with little presence in renal tubular cells [13]. Emerging evidences suggest that PMAT is involved in cellular uptake of endogenous amines as well as tissue-specific transport of xenobiotic organic cations [12,14,15].

The human and rodent PMAT proteins consist of 528–530 residues with a long cytoplasmic N-terminus [5,14]. At the protein level, human and rodent PMATs exhibit a low overall sequence identity (~20%) to the ENTs (i.e. ENT1-3) with the most divergent regions in the hydrophilic termini and loop regions. In the transmembrane (TM) regions, sequence identity significantly increases (up to 35–40%). Despite their distinct substrate profiles (i.e. organic cations versus nucleosides), previous studies suggest PMAT and ENTs share a similar protein structure with a common 11 TM membrane topology [16,17]. The major substrate recognition sites in PMAT and the ENTs are both located in the N-terminal half (TM1-6), and transplanting TM1-6 of PMAT into hENT1 converted hENT1 from a nucleoside transporter to an organic cation transporter [17]. Recent mutational analyses further identified several residues (Y85, Y112, E206, T220) in TM1, 2 and 5 of PMAT critical for substrate recognition and translocation [16,17]. Interestingly, these residues are located at or close to the TM regions or residues that are known to be important for nucleoside transport in the ENTs [16,17].

A well known characteristic of mammalian ENT1 and 2 proteins is their differential sensitivities to inhibition by classic nucleoside transporter inhibitors including nitrobenzylmercaptopurine riboside (NBMPR) and the coronary vasodilator drugs such as dilazep and dipyridamole [18–21]. Mammalian ENT1 proteins are highly sensitive to NBMPR (K_d = 1–10 nM) whereas the ENT2 transporters only become sensitive to NBMPR at micromolar concentrations (> 10 μM) [1,2]. Moreover, human and mouse ENT2 proteins are 2–3 orders of magnitude less sensitive to inhibition by dilazep and dipyridamole than ENT1 proteins, whereas both rat isoforms (rENT1 and rENT2) are insensitive to these inhibitors [22–24]. Previously, residue 33, predicted to lie at the extracellular end of TM 1 in hENT1 and hENT2, was shown to be a functionally important component of the binding sites for dilazep, dipyridamole, and nucleosides for both transporters [25,26]. In particular, a methionine residue at this position (e.g. Met33 in hENT1 and mENT1) facilitates high affinity interaction with dilazep and dipyridamole, whereas an isoleucine residue (i.e. Ile33 in hENT2, mENT2 and rENT1/2) confers low affinity interaction [22–26]. Substitution of

Ile33 with Met in hENT2 greatly enhanced its binding affinity to nucleosides, dilazep and dipyridamole, but not NBMPR [25,26]. Recent work in our laboratory revealed that like hENT2, human PMAT retains the low affinity interaction sites for classic ENT inhibitors [6]. NBMPR, dipyridamole, and dilazep inhibited PMAT-mediated MPP^+ uptake with K_i values that are similar or close to those of hENT2 but are 3–4 orders higher than those reported for hENT1 [6]. Interestingly, multiple sequence alignment revealed that similar to the ENT2 proteins, an isoleucine residue is conserved among human and rodent PMATs at position 89, which is equivalent to residue 33 in ENT1/2 (Fig.1). In the present study, we examined the role of I89 in PMAT-mediated organic cation transport and its interaction with the classic ENT inhibitors NBMPR, dilazep and dipyridamole.

2. Material and Methods

2.1. Materials

[^{3}H]MPP^+ (85 Ci/mmol) was obtained from American Radiolabeled Chemicals, Inc. (St. Louis, MO). Nitrobenzylmercaptopurine riboside (NBMPR), dilazep and dipyridamole were obtained from Sigma-Aldrich (St. Louis, MO). All other chemicals were obtained from Sigma-Aldrich (St. Louis, MO).

2.2. Generation of I89M mutant construct and stable expression in MDCK cells

We used the yellow fluorescence protein (YFP)-tagged wild-type (WT) human PMAT [5] as a template to construct the I89M mutant by site-directed mutagenesis using the QuickChange kit (Stratagene, La Jolla, CA). YFP was tagged at the N-terminus of WT PMAT and our previous studies showed that YFP tagging had no effect on the substrate selectivity or kinetic behavior of the transporter [16,17]. The sequence of I89M mutant was confirmed by direct DNA sequencing in the Department of Biochemistry at the University of Washington. WT PMAT, I89M mutant and the empty vector pEYFP-C1 were transfected into MDCK cells using Lipofectamine 2000 transfection reagent (Invitrogen, Carlsbad, CA). Transfected cells were selected in minimal essential medium containing 10% fetal bovine serum and G418 at 1000 μg/ml for 2–3 weeks. Fluorescence-positive cells were then purified with a FACS Vantage SE sorter (BD Biosciences, Bedford, MA) at the Cell Analysis Center at the University of Washington. Sorted cells were cultured and maintained in minimal essential medium containing G418 (200 μg/ml). For subsequent uptake and localization studies, cells were seeded on 24- or 6-well plates and cultured for 2–3 days until 90–100% confluent. Our previous studies showed that under these culture conditions, MDCK cells were not polarized [12]. There was also minimal endogenous PMAT activity in MDCK cells under our study conditions [13].

2.3. Confocal fluorescence microscopy

To determine the cellular localization of the YFP-tagged WT PMAT and I89M mutant, stably transfected cells were grown on top of microscope cover glass in six-well plates (Falcon, BD Biosciences, Bedford, MA) for 2–3 days until confluent. Cells were mounted onto microscope glass slides with Fluoromount-G (Electron Microscopy Sciences, Hatfield, PA) and images were visualized and captured by excitation at 488 nm and emission at 515 nm with a Leica SP1 confocal microscope equipped with an argon laser as the light source at the Keck Microscopy Facility at the University of Washington.

2.4. Cell surface biotinylation and western analysis

Stably transfected cells were seeded onto 60 mm plates and cultured for 2–3 days until confluent. Cells were washed twice with 3 mL of ice-cold PBS/CM [138 mM NaCl, 2.7mM KCl, 8mM Na_2HPO_4, 1.5mM KH_2PO_4, 0.1mM $CaCl_2$, and 1mM $MgCl_2$ (pH 8.0)] and then incubated (20 min twice at 4°C with gentle shaking) with 1 mL of ice-cold PBS/CM

containing a freshly prepared membrane-impermeable biotinylation reagent sulfo-NHS-SS-biotin (0.5 mg/mL) (Pierce, Rockford, IL). Unreacted NHS-SS-biotin was quenched by first rinsing the cells with 3 mL of PBS/CM containing 100 mM glycine and then further incubated at 4°C with the same solution for an additional 20 min. Cells were solubilized on ice via incubation in 1mL of lysis buffer containing 20 mM Tris, 150 mM NaCl, 1 mM EDTA, 1% Triton X-100, 1 mM phenylmethanesulfonyl fluoride, and Protease Inhibitor Cocktail (Roche, USA) for 1 h with occasional vortexing. Total protein concentrations were measured in supernatants and lysates containing the same amount of total protein were incubated with 50 μL of UltraLink Immobilized NeutrAvidin protein (Pierce, Rockford, IL) to pull down membrane proteins. Membrane fraction (pulled down) and cytosolic fraction (non pulled down) proteins were then analyzed by Western blotting with a mouse monoclonal anti-YFP antibody (JL-8) (BD Biosciences, Bedford, MA) at a 1:1000 dilution, and horseradish peroxidase-conjugated goat anti-mouse IgG (1:20000 dilution). Chemiluminescent signals were detected by SuperSignal West Pico Chemiluminescent Substrate (Pierce, Rockford, IL) followed by exposure to X-ray films. Band intensity was quantified by densitometry using ImageQuant (Molecular Dynamics, Sunnyvale, CA). Double bands at the expected molecular size (~75 kDa) were observed for both YFP-tagged WT PMAT and I89M mutant proteins, which could be due to differential glycosylation of the PMAT proteins [16,17].

2.5. Functional characterization in MDCK cells

Stably transfected cells were seeded in 24-well plates and allowed to grow for 2–3 days until ~90–100% confluent. For uptake studies, growth medium was aspirated and cells were rinsed once with Krebs-Ringer-Henseleit (KRH) buffer [5.6mM glucose, 125mM NaCl, 4.8mM KCl, 1.2mM KH_2PO_4, 1.2mM $CaCl_2$, 1.2mM $MgSO_4$, and 25 mM HEPES (pH 7.4)] and preincubated in KRH buffer for 15min at 37°C. Cells were than incubated in KRH buffer containing various concentrations of a [^{3}H]-labeled MPP^+ for 1 min at 37°C for the transport assay. Uptake was terminated by aspirating the uptake solution and washing the cells three times with ice-cold KRH buffer. Cells were solubilized with 0.5 mL of 1 N NaOH and neutralized with 0.5 mL of 1 N HCl. Liquid scintillation counting was used to quantify radioactivity in the cell lysate. Uptake in each well was normalized to its protein concentration as measured by the Pierce BCA protein assay kit (Pierce, Rockford, IL). For inhibition studies, cells were incubated at 37°C for 1 min in KRH buffer containing [^{3}H]MPP^+ (1 μM) and in the absence or presence of an inhibitor at various concentrations. Uptake was terminated by washing the cells three times with ice-cold KRH buffer and samples were assayed as described above.

2.6. Helical wheel analysis

Helical wheel analysis was done using HelixWheel on the EXPASY molecular biology server and subsequently transposed onto a helical wheel template. The transmembrane domain was assumed to be a standard α-helix (3.6 residues/helical turn). Residues in TM 1 were plotted every 100° around the center of a circle with the projection of the residues locations shown on a plane perpendicular to the helical axis. Hydrophobicity and hydrophilicity were assigned according to the consensus scale of Eisenberg et al. [27].

2.7. Data analysis

All uptake experiments were performed in triplicate and repeated two to four times. Data were expressed as mean ± S.D. from three independent experiments (n=3) with different cell passages. For MPP^+ transport kinetic studies, transporter-specific uptake at each data point was calculated by subtracting corresponding background uptake in vector (pEYFP-C1)-transfected cells. For kinetics studies, data were fitted to the Michaelis-Menten equation $V = V_{max}[S]/(K_m+[S])$, where V is the transport rate and [S] is the substrate concentration.

Kinetic parameters were determined by nonlinear least-squares regression fitting as described previously [5,7]. For inhibition studies, all experiments were performed in triplicate in three different wells on the same plate and repeated three times. IC_{50} values are given as mean ± S.D. from parameters obtained from three independent experiments (n=3) with different cell passages. The half-maximal inhibitory concentration (IC_{50}) was determined by fitting total uptake data in WT PMAT or I89M mutant expressing cells to the equation $V = V_0 + (V_{max} - V_0)/[1 + (I/IC_{50})^{nH}]$, where V is the rate of uptake of MPP^+ in the presence of the inhibitor, V_0 is the residual non-inhibitable baseline value, Vmax is the rate of uptake of MPP^+ in the absence of inhibitor, I is the inhibitor concentration, and nH is the Hill coefficient. Where applicable, p values were obtained through Student's t-test.

3. Results

3.1. MPP^+ transport kinetics of WT PMAT and I89M mutant

At position 33, residue Met (hENT1) and Ile (hENT2) have been shown to be important for hENT1/2 nucleoside transport function and their interactions with coronary vasodilators [25,26]. By sequence alignment analysis, we found that at the corresponding positions of M33 (hENT1) and I33 (hENT2), PMAT possesses an isoleucine residue at position 89 (Fig 1). This residue is conserved among PMATs from various species. To examine whether I89 is involved in interaction with substrates and/or inhibitors, we substituted isoleucine in PMAT to its counterpart in hENT1, methionine. YFP-tagged I89M mutant was constructed and stably expressed in MDCK cells. The transport kinetics of this mutant was analyzed by uptake studies using MPP^+, a prototype organic cation substrate for PMAT [5]. Compared to WT PMAT, I89M substitution produced a ~2.7-fold decrease in maximal velocity (Vmax), with minimal change in apparent binding affinity (Km) (Fig. 2 and Table 1). As a result, a corresponding 3.7-fold decrease in transport efficiency (Vmax/Km) towards MPP^+ was obtained (Table 1). The decreased Vmax of I89M mutant in MPP^+ uptake may suggest impairment in transporter function. Alternatively, the methionine substitution could have affected membrane trafficking and surface expression of the transporter.

3.2. Membrane expression and localization of I89M mutant

To delineate the mechanisms underlying the reduced Vmax in MPP^+ uptake observed in I89M mutant, cellular localization of WT PMAT and I89M mutant was visualized by confocal microscopy, and their plasma membrane expression levels were determined by cell surface biotinylation followed by Western blot analysis. As shown in Figure 3A, both WT PMAT and I89M mutant showed a predominant localization on the plasma membrane in MDCK cells. In contrast, cells transfected with the vector control (EYFP-C1) exhibited diffused fluorescence of YFP throughout the cytoplasm. Western blot analysis of membrane protein expression showed that WT PMAT and I89M mutant were expressed at similar levels at the cell surface (Fig. 3B). There was no detectable band on plasma membrane in vector-transfected cells. In addition, immunoblotting showed no detectable PMAT protein in unbound intracellular fractions prepared from WT and mutant cell lines, indicating no significant intracellular accumulation of WT PMAT or I89M mutant proteins (Fig. 3B). These data suggest that the decreased transport activity in I89M mutant cell line (Fig. 2) is not due to impaired protein stability or membrane trafficking, but reflects a change in the intrinsic catalytic activity of the transporter.

3.3 Sensitivity to NBMPR, dilazep, and dipyridamole

Previously Visser et al. showed that M33 in hENT1 and I33 in hENT2 are the key residues influencing transporter sensitivity to dilazep and dipyridamole, but not NBMPR [25]. To investigate whether the equivalent residue I89 in PMAT also plays a role in PMAT's interaction with classic ENT inhibitors, we determined the inhibitory effect of NBMPR,

dilazep and dipyridamole on MPP^+ uptake mediated by WT PMAT and I89M mutant. The IC_{50} values of each compound are summarized in Table 2. Our result showed that replacing Ile with Met at position 89 of PMAT increased the transporter's sensitivity to dilazep by ~2.5 fold. In contrast, no significant changes were observed in inhibitions by NBMPR or dipyridamole (Table 2).

3.4. Helical wheel analysis

I89 is predicted to be located at the extracellular end of TM 1 of PMAT, which is close to a key residue (Y85) previously identified as important for substrate recognition and transport (Fig. 4A) [16]. Recent homology-based modeling of *P. falciparum* ENT1 (PfENT1) transporter suggests that TM1 participates in the formation of the permeant translocation pathway and its α-helical structure extends beyond the lipid bilayer [28]. The overall protein sequence similarity between human PMAT and PfENT1 is ~30%. For the TM1 region, sequence alignment showed 19% identify and 48% similarity (Fig. 4B). Assuming a TM structure similar to PfENT1, I89 may be located on a extended α-helix facing the substrate permeation pathway in PMAT. To seek further evidence, we performed helical wheel analysis on residues 72–89 in TM1 of PMAT. The result revealed that I89 may be located in close proximity to Y85, a functionally important residue, on a transmembrane α-helical structure (Fig. 4C).

4. Discussion

Previous structure-function relationship studies revealed that despite their distinct substrate specificity, mammalian PMAT and ENT proteins share a similar architecture with major substrate recognition sites residing in the N-terminal half (TM1–6) [17,29,30]. In both ENTs and PMAT transporters, mutational analyses have suggested that TMs 1, 2 and 5 are important components of the substrate permeation pathway and contain residues important for substrate recognition and translocation [16,17,31–34]. Similar to ENT2, PMAT also retains the low affinity interaction sites for classic ENT inhibitors such as dilazep, dipyridamole, and NBMPR [6]. Previous analysis of hENT1 and hENT2 identified that residue 33 on TM1 is a functionally important component of the binding sites for dilazep, dipyridamole, and nucleosides for these transporters [25,26]. Interestingly, similar to ENT2, an Ile residue is conserved among human and rodent PMATs at position 89, which is the equivalent position of residue 33 in ENT1/2 (Fig. 1). To elucidate the role of I89 in PMAT function, we substituted Ile89 in WT PMAT with Met and characterized the mutant's transport kinetics towards organic cation substrate and its interaction with classic nucleoside transporter inhibitors.

Stable expression of YFP-tagged I89M mutant in MDCK cells resulted in normal cell surface expression (Fig. 3A). Western blot analysis of plasma membrane proteins further demonstrated that cell surface expression level of I89M mutant is comparable to that of WT PMAT (Fig. 3B), and there was no significant intracellular accumulation of WT and mutant proteins in the MDCK cells. Detailed kinetic analysis revealed that while the apparent binding affinity (Km) for MPP^+ was similar between WT PMAT and I89M mutant, the latter showed a much reduced maximal velocity (Vmax) (Fig. 2 and Table 1). Since the mutant showed normal plasma membrane expression and protein stability, the reduced Vmax should be due to a decreased turnover rate (kcat) in the mutant transporter. These kinetic characteristics suggest that residue I89 may not be directly involved in MPP^+ binding, but it influences other processes in the transport cycle, such as membrane translocation, substrate release, and/or returning of the empty transporter to its original state.

Recently, crystal structures were solved for several prokaryote transporters in the major facilitator superfamily (MFS) including the *Escherichia coli* lactose transporter LacY,

glycerol 3-phosphate transporter GlpT, and the *Aquifex aeolicus* leucine transporter LeuTAa [35–37]. These three-dimensional structures revealed that α-helix traversing the membrane can be tilted and longer than predicted or extend beyond the lipid bilayer [35–38]. Based on the crystal structure of GlpT [36], a structural model was proposed for *P. falciparum* ENT1 [28], which suggests that TM1 is an extended α-helix that participates in the formation of the permeant translocation pathway in the ENTs. PfENT1 and PMAT have a similar predicted secondary structure with 11 transmembrane domains, an intracellular amino and an extracellular carboxyl terminus as well as a long intracellular loop between transmembrane domains 6 and 7 [5,39]. The sequence similarity in TM1 between human PMAT and PfENT1 is ~48%. Assuming a similar three dimensional structure and an extended helical structure for TM1 in PMAT, I89 will be located in close proximity to Y85 on the same face of the α-helix (Fig. 4C). Our previous analysis showed that Y85 is directly involved in substrate recognition, and may interact with aromatic moieties commonly found in PMAT substrates via π-π interactions [16]. Together, these data suggest that I89 in PMAT may occupy a position that is close to the substrate recognition and permeation pathway. Nevertheless, it should be pointed out that our interpretation of the spatial relationship between I89 and Y85 on TM1 is purely hypothetical and requires the assumption that the TM1 helix extends to residue 89.

ENT1 and ENT2 are the pharmacological targets for the vasodilators dilazep and dipyridamole [19–21]. Dilazep and dipyridamole are believed to bind to a common site in ENT1/2 proteins that is different from the NBMPR-binding site [25,26,40]. Previous structure-function analyses of ENT1/2 transporters suggest that residue 33 is an important component of the binding sites for dilazep and dipyridamole. Substitution of Ile33 in hENT2 with Met renders the transporter 10 times more sensitive to dilazep and dipyridamole [25]. Recent work in our laboratory revealed that like hENT2, human PMAT retains the low affinity interaction binding to NBMPR, dipyridamole, and dilazep [6]. To investigate whether I89 affects the binding property of PMAT with ENT inhibitors, we determined the inhibition potency of NBMPR, dilazep and dipyridamole on MPP^+ transport mediated by WT PMAT and the I89M mutant. Our results showed that I89M mutant is more than twice as sensitive as WT PMAT to inhibition by dilazep (Table 2). The data suggest that I89 may directly interact with dilazep, and its substitution with the sulfur-containing and less hydrophobic Met residue further enhanced the interaction between dilazep with its binding pocket. In contrast, the Ile89Met substitution had no effect on PMAT's sensitivity towards dipyridamole. Dipyridamole may interact with a different set of residues within a common binding site that also accommodates dilazep. Alternatively, it may interact with PMAT at a separate binding site(s) from that of dilazep. It would be interesting to examine whether dilazep and dipyridamole share the same binding site and affect each other's binding by performing displacement binding assay using radio-labeled drugs in the WT and mutant cell lines. However, radio-labeled dilazep and dipyridamole are not available at the moment and we were unable to carry out such studies.

The relatively small effect of the Ile89Met substitution in PMAT on its interaction with coronary vasodilators is in contrasts with the dramatic effect produced at the equivalent position in hENT2. The corresponding Ile-to-Met mutation in hENT2 resulted in >10-fold increase in transporter sensitivity to both dilazep and dipyridamole [25]. For PMAT, Ile-to-Met mutation increased dilazep binding by ~2.5 fold, but had no effect on dipyridamole binding affinity. Furthermore, the substitution affected hENT2 in nucleoside binding (Km), but affected PMAT in Vmax for organic cation transport. These data suggest distinct role of this residue in substrate transport and inhibitor binding in PMAT as compared to ENT2. It should be noted that despite of their significant similarities in overall protein architecture and low affinity binding to coronary vasodilators, PMAT and ENT2 transport two entirely different classes of substrates. As the organic cations (e.g. MPP^+) and nucleosides have very

different chemical features, amino acid residues with different physicochemical properties are likely to be involved in direct binding with the two different types of substrates in the binding pockets of these transporters. This notion has been supported by our previous studies where all residues (e.g. Y85, Y112 and E206) identified critical for organic cation binding in PMAT are substituted by a different residue in the ENTs at the equivalent position [16,17]. Conversely, the same Ile residue in hENT2 involved in nucleoside substrate binding (as reflected by a Km change) appears to be delegated with a different role in the organic cation transport cycle as discussed earlier. For the same reason, it may not be surprising to see that the Ile-to-Met mutation produced different effect in PMAT's interaction with dipyramidole and dilazep. The data suggests substantial differences between PMAT and ENT2 in their binding mechanisms to dilazep and dipyridamole. Future investigations, including substitution with other amino acid residues and analysis of nearby residues, will help define the chemical and structural natures of Ile89 and nearby residues in PMAT interaction with the coronary drugs.

In summary, we have identified I89 as an important residue for PMAT function and its interaction with dilazep. Along with previous data, our study further suggests the involvement of TM1 of PMAT in forming the substrate permeation pathway for organic cation substrates. I89 may not be directly involved in substrate binding, but it influences the catalytic activity of the transporter. Our data also suggests that I89 may form part of the low-affinity binding site for the coronary vasodilators located close to the substrate binding pocket. However, it is also possible that the observed changes in substrate transport and inhibitor binding of I89M mutant are due to an indirect effect produced by an overall change in the tertiary structure of the mutant transporter protein. This alternative hypothesis is difficult to exclude in the absence of a true three-dimensional structure of the transporter. Nevertheless, combined with our previous structure-function analysis on PMAT and the observed structural similarities between PMAT and ENTs, the current study warrants further investigation of I89 and TM1 in PMAT function and its interaction with classic ENT inhibitors.

Acknowledgments

This work is supported by the National Institutes of Health Grant GM066233.

Abbreviations

PMAT	Plasma membrane monoamine transporter
SLC29	solute carrier 29
SLC22	solute carrier 22
MPP^+	1-methyl-4-phenylpyridinium
ENT	Equilibrative nucleoside transporter
Vmax	maximal transport velocity
Km	apparent binding affinity
OCT	organic cation transporter
NBMPR	Nitrobenzylmercaptopurine Riboside
YFP	yellow fluorescence protein
MDCK	Madin-Darby canine kidney
FACS	Fluorescence Activated Cell Sorting

TM transmembrane domain

References

1. Baldwin SA, Beal PR, Yao SY, King AE, Cass CE, Young JD. The equilibrative nucleoside transporter family, SLC29. Pflugers Arch. 2004; 447:735–43. [PubMed: 12838422]
2. Kong W, Engel K, Wang J. Mammalian nucleoside transporters. Curr Drug Metab. 2004; 5:63–84. [PubMed: 14965251]
3. Baldwin SA, Yao SY, Hyde RJ, Ng AM, Foppolo S, Barnes K, et al. Functional characterization of novel human and mouse equilibrative nucleoside transporters (hENT3 and mENT3) located in intracellular membranes. J Biol Chem. 2005; 280:15880–7. [PubMed: 15701636]
4. Govindarajan R, Leung GP, Zhou M, Tse CM, Wang J, Unadkat JD. Facilitated mitochondrial import of antiviral and anticancer nucleoside drugs by human equilibrative nucleoside transporter-3. Am J Physiol Gastrointest Liver Physiol. 2009; 296:G910–22. [PubMed: 19164483]
5. Engel K, Zhou M, Wang J. Identification and characterization of a novel monoamine transporter in the human brain. J Biol Chem. 2004; 279:50042–9. [PubMed: 15448143]
6. Zhou M, Duan H, Engel K, Xia L, Wang J. Adenosine transport by plasma membrane monoamine transporter: reinvestigation and comparison with organic cations. Drug Metab Dispos. 2010; 38:1798–805. [PubMed: 20592246]
7. Engel K, Wang J. Interaction of organic cations with a newly identified plasma membrane monoamine transporter. Mol Pharmacol. 2005; 68:1397–407. [PubMed: 16099839]
8. Zhou M, Xia L, Wang J. Metformin transport by a newly cloned proton-stimulated organic cation transporter (plasma membrane monoamine transporter) expressed in human intestine. Drug Metab Dispos. 2007; 35:1956–62. [PubMed: 17600084]
9. Koepsell H, Lips K, Volk C. Polyspecific organic cation transporters: structure, function, physiological roles, and biopharmaceutical implications. Pharm Res. 2007; 24:1227–51. [PubMed: 17473959]
10. Wright SH, Dantzler WH. Molecular and cellular physiology of renal organic cation and anion transport. Physiol Rev. 2004; 84:987–1049. [PubMed: 15269342]
11. Itagaki S, Ganapathy V, Ho HT, Zhou M, Babu E, Wang J. Electrophysiological Characterization of the Polyspecific Organic Cation Transporter Plasma Membrane Monoamine Transporter. Drug Metab Dispos. 2012
12. Xia L, Engel K, Zhou M, Wang J. Membrane localization and pH-dependent transport of a newly cloned organic cation transporter (PMAT) in kidney cells. Am J Physiol Renal Physiol. 2007; 292:F682–90. [PubMed: 17018840]
13. Xia L, Zhou M, Kalhorn TF, Ho HT, Wang J. Podocyte-specific expression of organic cation transporter PMAT: implication in puromycin aminonucleoside nephrotoxicity. Am J Physiol Renal Physiol. 2009; 296:F1307–13. [PubMed: 19357181]
14. Dahlin A, Xia L, Kong W, Hevner R, Wang J. Expression and immunolocalization of the plasma membrane monoamine transporter in the brain. Neuroscience. 2007; 146:1193–211. [PubMed: 17408864]
15. Zhou M, Engel K, Wang J. Evidence for significant contribution of a newly identified monoamine transporter (PMAT) to serotonin uptake in the human brain. Biochem Pharmacol. 2007; 73:147–54. [PubMed: 17046718]
16. Ho HT, Wang J. Tyrosine 112 is essential for organic cation transport by the plasma membrane monoamine transporter. Biochemistry. 2010; 49:7839–46. [PubMed: 20687515]
17. Zhou M, Xia L, Engel K, Wang J. Molecular determinants of substrate selectivity of a novel organic cation transporter (PMAT) in the SLC29 family. J Biol Chem. 2007; 282:3188–95. [PubMed: 17121826]
18. Baldwin SA, Mackey JR, Cass CE, Young JD. Nucleoside transporters: molecular biology and implications for therapeutic development. Mol Med Today. 1999; 5:216–24. [PubMed: 10322314]

19. Griffith DA, Jarvis SM. Nucleoside and nucleobase transport systems of mammalian cells. Biochim Biophys Acta. 1996; 1286:153–81. [PubMed: 8982282]
20. Hammond JR. Interaction of a series of draflazine analogues with equilibrative nucleoside transporters: species differences and transporter subtype selectivity. Naunyn Schmiedebergs Arch Pharmacol. 2000; 361:373–82. [PubMed: 10763851]
21. Van Belle H. Nucleoside transport inhibition: a therapeutic approach to cardioprotection via adenosine? Cardiovasc Res. 1993; 27:68–76. [PubMed: 8458034]
22. Kiss A, Farah K, Kim J, Garriock RJ, Drysdale TA, Hammond JR. Molecular cloning and functional characterization of inhibitor-sensitive (mENT1) and inhibitor-resistant (mENT2) equilibrative nucleoside transporters from mouse brain. Biochem J. 2000; 352(Pt 2):363–72. [PubMed: 11085929]
23. Ward JL, Sherali A, Mo ZP, Tse CM. Kinetic and pharmacological properties of cloned human equilibrative nucleoside transporters, ENT1 and ENT2, stably expressed in nucleoside transporter-deficient PK15 cells. Ent2 exhibits a low affinity for guanosine and cytidine but a high affinity for inosine. J Biol Chem. 2000; 275:8375–81. [PubMed: 10722669]
24. Yao SY, Ng AM, Muzyka WR, Griffiths M, Cass CE, Baldwin SA, et al. Molecular cloning and functional characterization of nitrobenzylthioinosine (NBMPR)-sensitive (es) and NBMPR-insensitive (ei) equilibrative nucleoside transporter proteins (rENT1 and rENT2) from rat tissues. J Biol Chem. 1997; 272:28423–30. [PubMed: 9353301]
25. Visser F, Vickers MF, Ng AM, Baldwin SA, Young JD, Cass CE. Mutation of residue 33 of human equilibrative nucleoside transporters 1 and 2 alters sensitivity to inhibition of transport by dilazep and dipyridamole. J Biol Chem. 2002; 277:395–401. [PubMed: 11689555]
26. Visser F, Zhang J, Raborn RT, Baldwin SA, Young JD, Cass CE. Residue 33 of human equilibrative nucleoside transporter 2 is a functionally important component of both the dipyridamole and nucleoside binding sites. Mol Pharmacol. 2005; 67:1291–8. [PubMed: 15644498]
27. Eisenberg D, Wilcox W, McLachlan AD. Hydrophobicity and amphiphilicity in protein structure. J Cell Biochem. 1986; 31:11–7. [PubMed: 3722276]
28. Baldwin SA, McConkey GA, Cass CE, Young JD. Nucleoside transport as a potential target for chemotherapy in malaria. Curr Pharm Des. 2007; 13:569–80. [PubMed: 17346175]
29. Sundaram M, Yao SY, Ng AM, Griffiths M, Cass CE, Baldwin SA, et al. Chimeric constructs between human and rat equilibrative nucleoside transporters (hENT1 and rENT1) reveal hENT1 structural domains interacting with coronary vasoactive drugs. J Biol Chem. 1998; 273:21519–25. [PubMed: 9705281]
30. Yao SY, Ng AM, Vickers MF, Sundaram M, Cass CE, Baldwin SA, et al. Functional and molecular characterization of nucleobase transport by recombinant human and rat equilibrative nucleoside transporters 1 and 2. Chimeric constructs reveal a role for the ENT2 helix 5–6 region in nucleobase translocation. J Biol Chem. 2002; 277:24938–48. [PubMed: 12006583]
31. Endres CJ, Sengupta DJ, Unadkat JD. Mutation of leucine-92 selectively reduces the apparent affinity of inosine, guanosine, NBMPR [S6-(4-nitrobenzyl)-mercaptopurine riboside] and dilazep for the human equilibrative nucleoside transporter, hENT1. Biochem J. 2004; 380:131–7. [PubMed: 14759222]
32. Endres CJ, Unadkat JD. Residues Met89 and Ser160 in the human equilibrative nucleoside transporter 1 affect its affinity for adenosine, guanosine, S6-(4-nitrobenzyl)-mercaptopurine riboside, and dipyridamole. Mol Pharmacol. 2005; 67:837–44. [PubMed: 15557207]
33. Paproski RJ, Visser F, Zhang J, Tackaberry T, Damaraju V, Baldwin SA, et al. Mutation of Trp29 of human equilibrative nucleoside transporter 1 alters affinity for coronary vasodilator drugs and nucleoside selectivity. Biochem J. 2008; 414:291–300. [PubMed: 18462193]
34. SenGupta DJ, Lum PY, Lai Y, Shubochkina E, Bakken AH, Schneider G, et al. A single glycine mutation in the equilibrative nucleoside transporter gene, hENT1, alters nucleoside transport activity and sensitivity to nitrobenzylthioinosine. Biochemistry. 2002; 41:1512–9. [PubMed: 11814344]
35. Abramson J, Smirnova I, Kasho V, Verner G, Kaback HR, Iwata S. Structure and mechanism of the lactose permease of Escherichia coli. Science. 2003; 301:610–5. [PubMed: 12893935]

36. Huang Y, Lemieux MJ, Song J, Auer M, Wang DN. Structure and mechanism of the glycerol-3-phosphate transporter from Escherichia coli. Science. 2003; 301:616–20. [PubMed: 12893936]

37. Yamashita A, Singh SK, Kawate T, Jin Y, Gouaux E. Crystal structure of a bacterial homologue of Na+/Cl−-dependent neurotransmitter transporters. Nature. 2005; 437:215–23. [PubMed: 16041361]

38. Henry LK, Defelice LJ, Blakely RD. Getting the message across: a recent transporter structure shows the way. Neuron. 2006; 49:791–6. [PubMed: 16543127]

39. Carter NS, Ben Mamoun C, Liu W, Silva EO, Landfear SM, Goldberg DE, et al. Isolation and functional characterization of the PfNT1 nucleoside transporter gene from Plasmodium falciparum. J Biol Chem. 2000; 275:10683–91. [PubMed: 10744765]

40. Visser F, Sun L, Damaraju V, Tackaberry T, Peng Y, Robins MJ, et al. Residues 334 and 338 in transmembrane segment 8 of human equilibrative nucleoside transporter 1 are important determinants of inhibitor sensitivity, protein folding, and catalytic turnover. J Biol Chem. 2007; 282:14148–57. [PubMed: 17379602]

Figure 1.

Multiple sequence alignment of mammalian PMATs and ENTs around the predicted TM1 region of hPMAT. I89 in hPMAT and its corresponding residues in PMAT orthologs and ENTs are highlighted in yellow for isoleucine (I) and red for methionine (M). I89 in hPMAT and corresponding residues in hENT1 and hENT2 are numbered. (r: rat; m: mouse; ca: canine; c: cattle; mac: macaques; h: human; rb: rabbit)

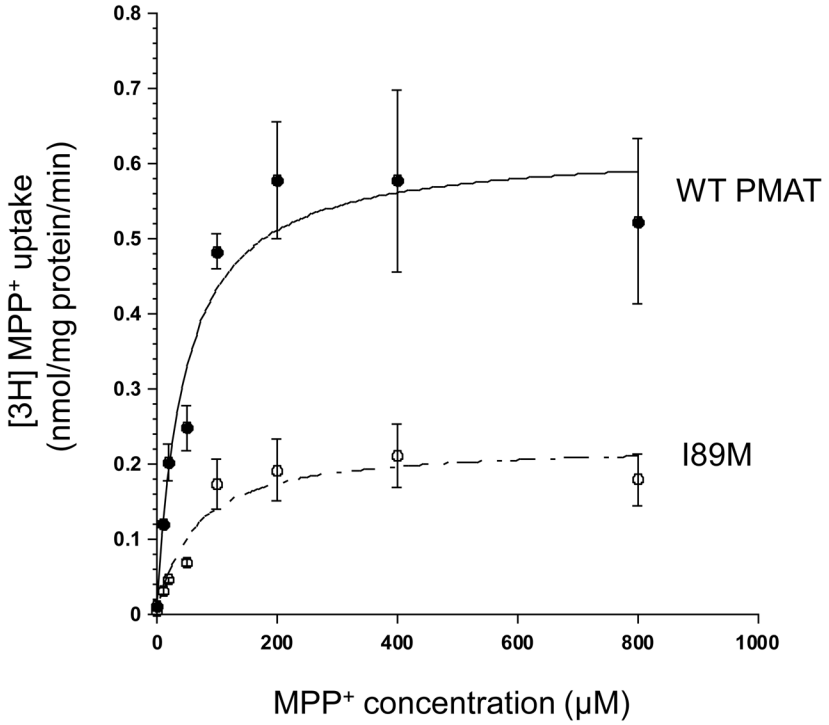

Figure 2.

Concentration-dependent transport of MPP^+ by WT PMAT and I89M mutant. EYFP-C1 vector-, WT PMAT- and I89M- stably transfected MDCK cells were incubated with varying concentrations of the substrates MPP^+ for 1 min at 37°C. Specific uptake was calculated by subtracting the uptake values in vector-transfected cells. WT PMAT (●) and I89M (○) concentration-dependent uptake were shown. Each value represents the mean ± S.D. from three independent experiments (n=3) with different cell passages. For each experiment, uptake was carried out in triplicates in three different wells on the same plate.

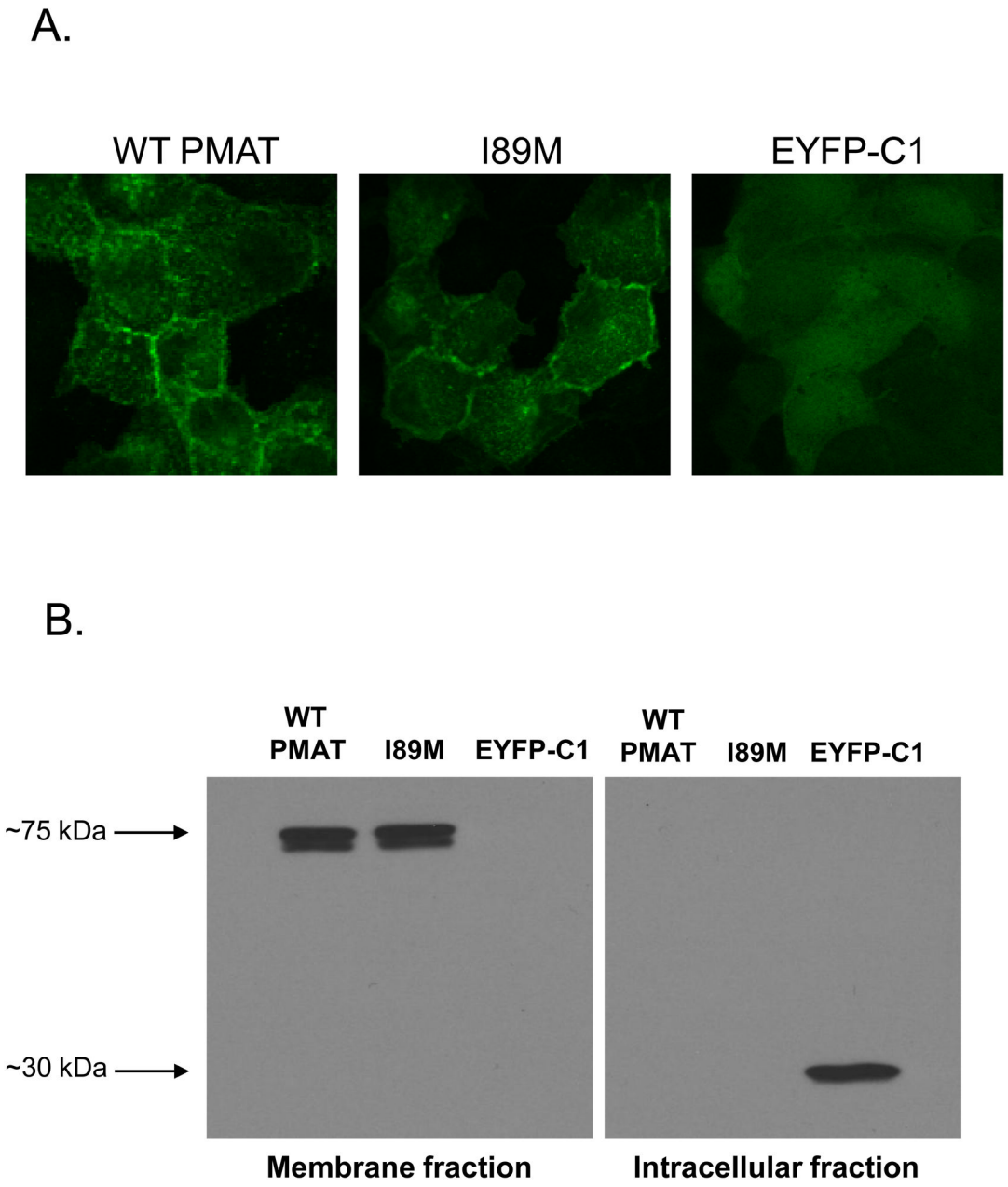

Figure 3.

(A) Confocal imaging of cellular localization of WT PMAT, I89M mutant and EYFP-C1 vector in stably transfected MDCK cells. (B) Plasma membrane expression (as detected by biotinylation) and intracellular expression (proteins not bound to the membrane-impermeable biotinylation reagent sulfo-NHS-SS-biotin) of WT PMAT, I89M mutant and EYFP-C1 vector followed by Western blot with an anti-yellow fluorescent protein (YFP) monoclonal antibody. Predicted molecular weight of YFP (~30 kDa) and YFP-tagged PMAT protein (~75 kDa) are indicated.

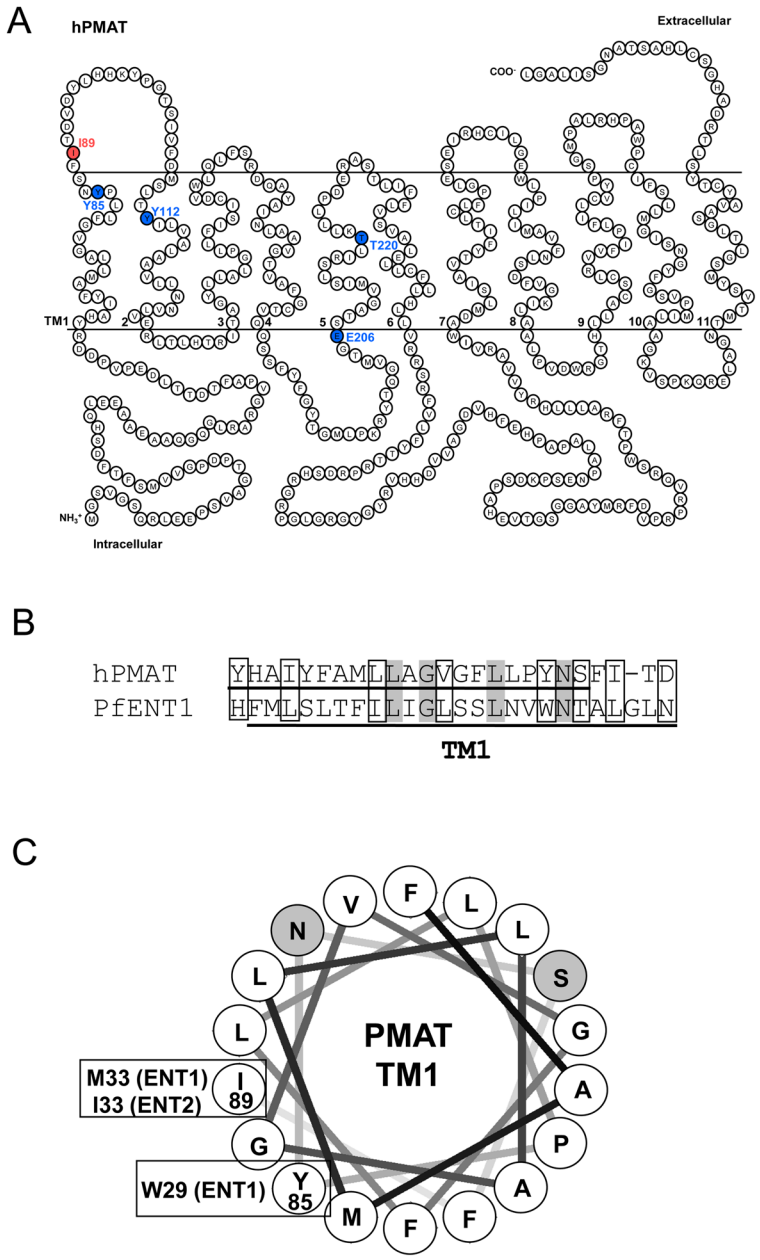

Figure 4.

(A) Proposed secondary structure of hPMAT. Position of I89 residue is highlighted in red. Previously identified functionally important residues are highlighted in blue. (B) Sequence comparison between hPMAT and PfENT1 in the predicted TM1 region. Identical amino acids are shaded, conserved amino acids are boxed. The predicted TM1 for hPMAT and PfENT1 are shown by solid lines below the aligned sequences. (h: human; Pf: *P. falciparum*). (C) Helical wheel analysis of TM1 of PMAT. The transmembrane domain is assumed to be standard α-helix and each residue is plotted every 100° around the center of a circle. The figure shows the projection of the positions of the residues on a plane perpendicular to the helical axis. Hydrophobic residues are shown in white, and hydrophilic residues are shown in gray. Functionally important residues previously identified in PMAT,

ENT1 and ENT2 with positions corresponding or close to I89 in PMAT are indicated in brackets.

Table 1

MPP^+ transport kinetics of WT PMAT and I89M mutant.

	Km (μM)	Vmax (nmol/mg protein/min)	Vmax/Km
WT PMAT	43.6 ± 13.2	0.62 ± 0.05 *	0.0142 ± 0.0044 **
I89M	60.1 ± 23.3	0.23 ± 0.02	0.0038 ± 0.0015

All experiments were performed in triplicate in three different wells on the same plate and repeated three times. Values were expressed as mean ± S.D. from parameters obtained from three independent experiments (n=3) with different cell passages.

* $p<0.01$ vs I89M value.

** $p<0.05$ vs I89M value.

Table 2

IC_{50} values of various compounds on MPP^+ uptake.

Inhibitors	IC_{50}(μM)	
	WT PMAT	I89M
NBMPR	16.8 ± 2.5	11.5 ± 5.1
Dilazep	16.6 ± 2.1 *	6.6 ± 0.5
Dipyridamole	2.8 ± 1.3	4.6 ± 1.8

Each compound was tested in both WT PMAT- and I89M- transfected MDCK cell lines. All experiments were performed in triplicate in three different wells on the same plate and repeated three times. IC_{50} values are given as mean ± S.D. from parameters obtained from three independent experiments (n=3) with different cell passages.

* $p<0.01$ vs I89M value.